Validation of non-destructive testing techniques for additive manufacturing

Joana Antunes
joana.ferreira.antunes@tecnico.ulisboa.pt

Instituto Superior Técnico, Universidade de Lisboa, Portugal

November 2019

Abstract

This work consolidates the application of both eddy current (EC) and ultrasonic (UT) techniques for the in-line inspection of defects on large Wire Arc Additive Manufacturing (WAAM) steel parts. WAAM technology is being recognized as one of the most cost-effective manufacturing processes for large part production in industries such as aerospace, oil and gas, architecture, renewable energies, among others. However, before WAAM can be successfully implemented in these sectors, non-destructive testing (NDT) systems must be developed in order to produce quality assured finished components.

Carbon-steel lacks investigation in the WAAM NDT field as progress on this topic was achieved mainly on allumium. This material faces many inspection challenges due to its ferromagnetic proprieties, surface texture and high temperatures during deposition. Regarding EC, a new customized probe was developed to reach higher penetration depths than its predecessors and overcome the magnetic limitations. In the UT field, a realistic computational model for phased array UT (PAUT) was designed to evaluate the waviness effect on defect detectability, which was experimentally validated. Moreover, the effect of using solder paste as UT couplant for high temperature inspection was also studied.

Experimental outcomes show the potential of both inspection methods for being used complementary in both non-ferromagnetic and ferromagnetic materials depending on part geometry. Both EC and UT techniques were able to detect defects on the required depths and the solder paste showed great potential to be used as a couplant on a realistic inspection scenario.

Keywords: Wire and arc additive manufacturing, non-destructive-testing, eddy current testing, ultrasonic testing.

1. Introduction

Additive Manufacturing (AM) is a technique in which parts are built layer by layer. This process is increasingly gaining relevance in the manufacturing industry and holds the potential to completely change the way products are designed and built in sectors such as aerospace, oil and gas, architecture, renewable energies, among others. Compared to other AM techniques for metals, Wire Arc Additive Manufacturing (WAAM) seems to be "one of the most promising techniques for fabricating large components with moderate complexity and relatively low costs", according to [4]. However, significant research is still required to reach reliable industrial implementation for part production. Before this technology becomes standard, one of the main aspects to address is the development of non-destructive techniques (NDT) to assure the quality of the parts produced.

According to [2], both ultrasonic (UT) and eddy current (EC) techniques have been identified has having the potential to be used in the in-line inspection of AM metal parts fabricated using WAAM. However, most of this previous research was centred on aluminium. On the other hand, carbon steel is one of the most accessible metals in the AM printing market, and can be used under different types of alloys making it highly attractive for industries with their own requirements. However, this material faces many inspection challenges due to its ferromagnetic proprieties, surface texture and high temperatures during deposition [5, 8]. That being said, the main focus of this work was the consolidation of the mentioned NDT techniques for the case of steel, as the use of this material implies surpassing many technological challenges before proper inspection.

2. Manufacture and characterization of samples

Before being able to evaluate the different NDT techniques, WAAM walls were deposited on the top of a substrate plate using ER70S-6 carbon-steel weld wire. Cold Metal Transfer (CMT) was used as the arc welding process, which is a modified

GMAW variant that "relies on controlled dip transfer mode mechanism to provide beads with good quality, lower thermal heat input and nearly without spatter", according to [6]. The motion of the torch was provided by a six-axis Kuka Robot.

The deposition parameters were selected in order to ensure structural integrity and overall acceptable surface texture in order to benefit inspection. The systematic procedure was conducted using a oscillation deposition strategy varying the Wire Feed Speed (WFS) and WFS/Travel Speed (TS) ratio. The addition of this last term serves to control the added material per unit length. The samples' microstrure was checked and radiographic testing was performed to ensure no defects were created during deposition.

Although most samples had an acceptable texture to the unaided eye, it is of great interest to minimize it as much as possible in order to avoid the extra step of machining the top of the walls. With this objective in mind, a triangular weaving deposition strategy was attempted, where the welding torch swings along the leading line. In the robot programming, there were two main parameters for the weaving motion of the torch, namely, amplitude (W_a) and weave length (W_l). Increasing these parameters leads to a more "spread" bead as increasing the W_a transversely stretches the welding pool while increasing the W_l tends to extend it. This leads to a flatter welding bead with a decreased contact angle. After optimizing the mentioned parameters, a *Stil Initial* chromatic confocal sensor was used to measure texture. A 1-D median filter on MATLAB was applied to the acquired data to reduce the noisesome results, which consequently reduced part of the roughness variations, meaning that the graphs obtained are an approximation of the waviness profile. Figure 1 shows the obtained results compared with the oscillation samples manufactured with the same welding parameters.

This results permitted to conclude that the triangular weaving deposition was beneficial for the samples' waviness when compared to the oscillation strategy. However, one can also see that the best results were obtained for the lowest WFS. According to [9], this can be explained by the fact that an increase of WFS tends to decrease surface quality due to the combining effects of the layer height and arc force.

Finally, the microstructure of the samples was analysed and no defects were detected. Both weaving and oscillation samples shared identical microconstituents on equivalent portions of the samples along with simillar grain size.

Identical samples to figure 1 a) and b) were used for the EC and UT inspection respectively.

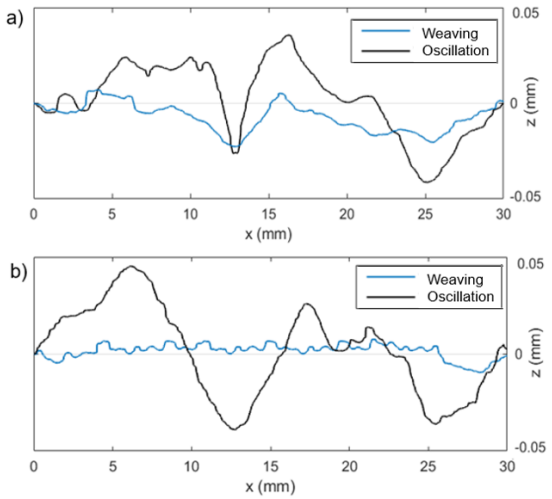

Figure 1: Weaving influence on waviness for different welding parameters: a) WFS = 3 m/min, WFS/TS = 10; b) WFS = 7 m/min, WFS/TS = 40.

3. Non-destructive testing techniques

3.1. Eddy Current testing

The development of customized EC IOnic probes [1] proved to surpass the limitations of its commercial predecessors when considering the in-line inspection of aluminium WAAM samples. Although these preliminary results represented an important step towards the development of NDT systems for WAAM, its important to access the capabilities of this inspection technique in steel and other ferromagnetic materials.

Materials which possess a high relative permeability value, $\mu_r \gg 1$, are called ferromagnetic materials because of their own innate ability to exhibit magnetic effects. In contrast to other substances, ferromagnetic materials are magnetized easily and in strong magnetic fields the magnetization does not return to its original value - hysteresis. In figure 2 one can see the standard depth of penetration, δ [m] which is presented as:

$$\delta_{(f,\mu,\sigma)} = \frac{1}{\sqrt{\pi \cdot f \cdot \mu \cdot \sigma}} \tag{1}$$

Where f [Hz] is the excitation frequency used, μ [H/m] is the magnetic permeability of the tested material, and σ [S/m] the electrical conductivity. Two different materials were considered: aluminium, with $\sigma \approx 30\%$ IACS and $\mu = 1$ H/m; mild-steel with $\sigma \approx 5\%$ IACS and $\mu = 2000$ H/m .

Although the values of μ and σ used were merely examples as both can vary depending on several conditions, one can observe that the standard depth of penetration in steel is almost 95% less that in aluminium due to the ferromagnetic characteristics of the first, confirming the importance of the magnetic characteristics for the effectiveness of the ECT method.

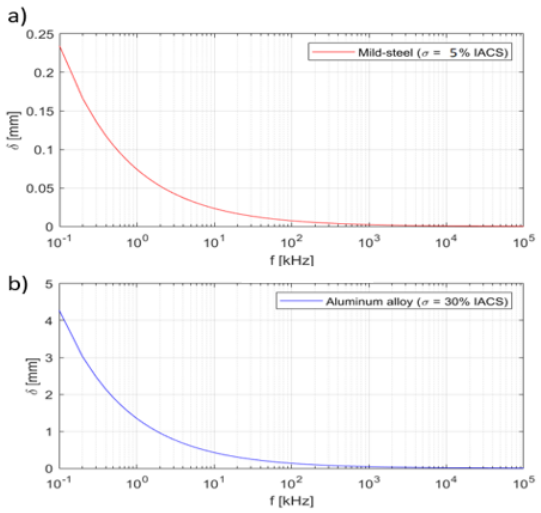

Figure 2: Standard penetration of aluminum (a) and mild-steel (b) in function of the frequency used.

The previously developed IOnic #3 probe [1] was put to test on a steel bar with a 3 mm diameter driller hole, 2 mm under the top surface. Although it detected the defect, the SNR was low and the results weren't as satisfactory as the previously obtained in aluminium. For this reason it was decided to further investigate on different EC Ionic probe designs and working principles, with the objective of developing a more promising model for the in-line inspection of WAAM steel parts.

3.1.1 Probe development

With the purpose of detecting internal defects in WAAM samples and improving the SNR while inspecting ferromagnetic materials: the Sideways Excitation Probe (SEP) was developed. This customized probe was designed under the hypothesis that an higher perturbation of the EC field would be achieved by having two ferrite cored excitation coils, one on each side of the sample, with the winding in the same direction. To back up this new design, numerical simulations based on finite element analysis (FEA) were performed to solve and illustrate the electromagnetic phenomena of the EC probes. The software used was ANSYS Electronics – Maxwell 3D.

The selected material for steel bar was steel with a bulk conductivity of 5.86 x 10^{-6} s/m and relative permeability of 3000 (the B-H curve effect was neglected). The bar had some curvature to its top surface in order to approximate the model to a typical WAAM surface, while ignoring the texture to simplify the analysis. The defect was a 350 µm x 5 mm (XZ) rectangle that went through all of the samples' width in the y direction. The results of this simulation for a frequency of 1 kHz are shown on figure 3.

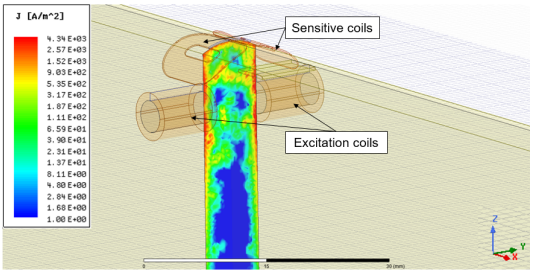

(a) Steel bar without defect.

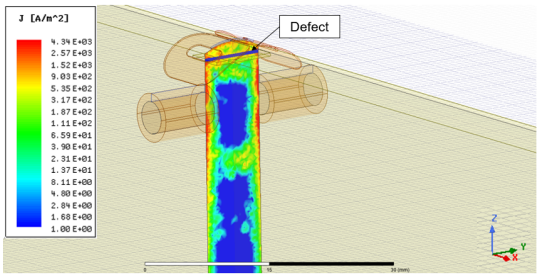

(b) Steel bar with 350 µm x 5 mm (XZ) rectangular defect through widht.

Figure 3: The magnitude of the component Y of the field $\vec{J}$ in the XZ plane for SEP probe using f = 1 kHz.

One can observe that the current density is focused all around the laterals and the top of the sample. The defect is clearly perturbed the EC flow as expected since this probe configuration concentrates the EC on the laterals of the bar. Due to the promising simulation results, a prototype of the SEP probe was 3D printed in Polylactic Acid (PLA) and the molds for the sensitive coils were made of Polyvinyl Alcohol (PVA), a water-soluble polymer that is dissolved after the sensitive coil winding around the mold is completed. The cores of the excitation coils were made of ferrite cylinders with 4 mm diameter. Two PLA screws were added for the possibility to adapt the gap between the excitation coils to the width of the inspection sample. This also allows to adapt the angle between the excitation and sensitive coils. The final design can be seen in figure 4.

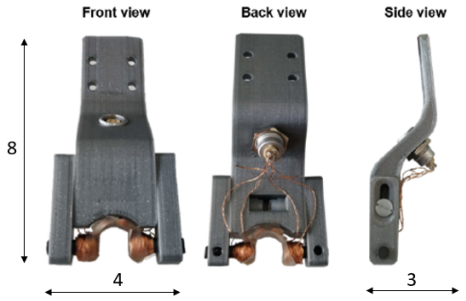

Figure 4: SEP probe final design. Dimensions in cm.

Similar to the simulation, the sensitive coils were 40 turns each wound up in opposite directions and

the excitation coils had both 200 turns wound up in the same direction. The SEP probes have a reflection absolution configuration therefore it is expected that a defect is signalized by only one peak.

Wire electrical discharge machining (WEDM) was used to create a 350 µm x 5 mm defect, identical to the last simulation. The slot's top was 2 mm below the surface of the sample and went throughout all of the wall's width, as shown on figure 5.

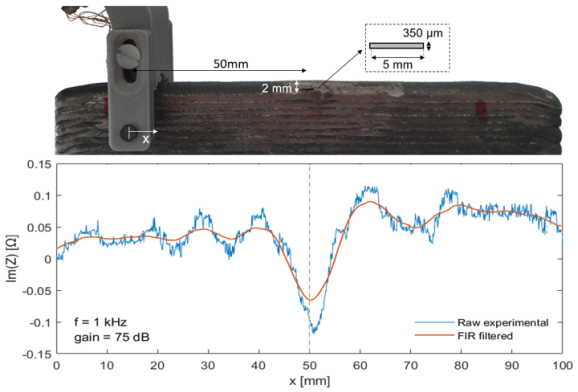

Figure 5: ECT results for defect 350 µm x 5 mm defect.

It can be observed that the probe detects the defect as a peak in the impedance is clear on the x = 50 mm mark. These results were accomplished by using a frequency of 1 kHz and a gain of 75 dB. After the successful result, this probe configuration was challenged by attempting to inspect an internal defect. To do so, the last WEDM defect was closed by welding each side of the WAAM wall using Tungsten Inert Gas (TIG). Chalk powder, a non-conductive material, was placed inside the slot before closing it. Radiographic testing was performed in order to verify if the defect was still present after the welding procedure.

The internal defect was then inspected using a wide range of frequencies. The best results were achieved for f = 1 kHz and 82 dB of gain, as seen in figure 6.

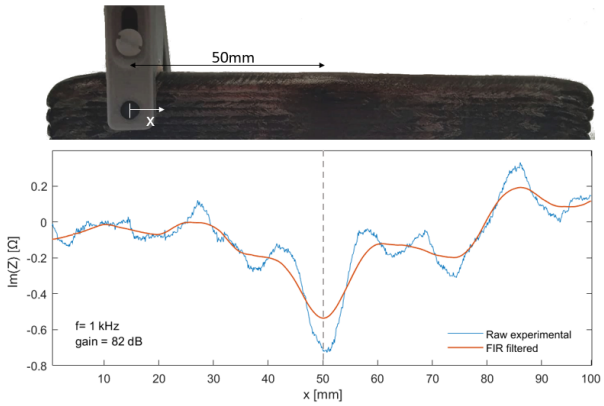

Figure 6: ECT results for an internal defect 350 µm thickness and 5 mm in length.

Similarly to the inspection of the open defect, the peak can be seen in the x = 50 mm mark but the SNR decreased, as expected. Although the impedance peak indicates a successful detection, the fact that the steel filler material used wasn't of the same exact steel as the WAAM wall might be influencing the results causing the impedance variation. Nevertheless, this new SEP probe design showed improvements in the detection capabilities of internal defects and ECT proved to be a promising solution for the in-line control of WAAM steel parts.

3.2. Ultrasonic testing

According to [3], phased array ultrasonic testing (PAUT) was indicated as one of the most promising techniques for the in-line inspection of WAAM parts. PAUT systems utilise multi-element probes, which are individually excited. By exciting each element in a controlled manner, a focused beam can be generated and steered by the use of proper software. Two and three dimensional views can be generated showing the sizes and locations of any flaws detected. The present work analysed two aspects of the PAUT inspection of WAAM produced parts in order to improve its capabilities: surface texture and coupling medium.

3.2.1 Inspection modeling

Regarding surface texture, one of the first objectives was developing a realistic PAUT inspection model on the commercial simulation and analysis software CIVA in order to understand the influence of waviness in inspection. CIVA^{TM} NDE is a simulation and analysis commercial software specifically developed for NDT applications, whence why it was used in this work. This software permits the control of a wide range of options from types of probes to different defect scattering models, allowing the prediction of various inspection techniques.

In order to introduce waviness into CIVA, several CAD models were experimented. The data from figure 1 was imported to Solidworks which created splines through the discrete points. This attempt was not successful as the data resolution was to high for CIVA to process. For a realistic inspection the mesh would have to be extremely refined leading to a unacceptably long computation time. For this reason, a simplified approach was used and a CAD surface was manually designed with a maximum height variation of 0.04 mm in 10 mm steps. Then, a parallelepiped CAD specimen was created with two halves having different surfaces: one planar and the other wavy, as seen in figure 7. Because of CIVA's comparative scale, having two different surfaces in the same specimen instead of two models permitted a direct comparison of the

inspection simulations results.

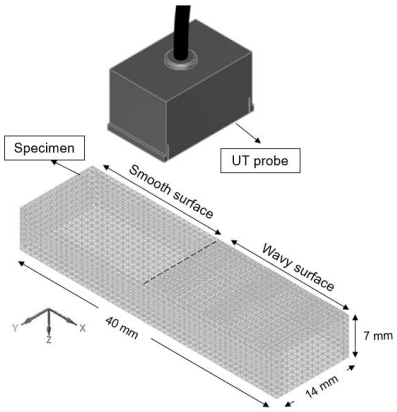

Figure 7: Final inspection model.

The chosen material for the specimen was isotropic carbon steel with density, ρ = 7.8 $\mathrm{g\,cm^{-3}}$ and longitudinal wave velocity of 5900 $\mathrm{m\,s^{-1}}$.

An immersion type probe with linear phased array pattern and 32 elements with flat focusing was selected. The chosen frequency was 5 MHz. Taking in consideration the average layer height in WAAM, single point focusing in the inspection plane was selected along the longitudinal axis Z = 2.5 mm as this was the region of interest. The uniform delay laws were calculated for longitudinal waves accounting for backwall reflection. Finally, a water path of 20 mm between the specimen and the UT probe was selected, with ρ = 1 $\mathrm{g\,cm^{3}}$ and primary wave velocity of 1483 $\mathrm{m\,s^{-1}}$. The attenuation laws were neglected both in the specimen and water medium, to simplify the analysis.

Having set most computation parameters, the probe active aperture was studied in order to optimize the number of elements needed for inspection. 12 elements were selected as the most promising aperture as the maximum pressure was focused on the region of interest and shortly distanced from the top surface (avoiding high amplitudes on the first echo which tend to camouflage the defects). Secondly two simulations were carried out placing the probe over the two different surfaces. The results of this beam computations are shown on figure 8.

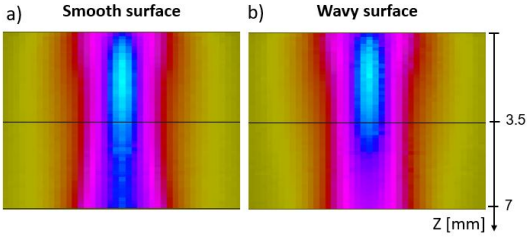

Figure 8: Visualization of the beam spread for different surface textures for 12 active elements.

The main difference between the two simulations can be seen in the 3.5 to 7 mm mark. One can clearly note a significant decrease in acoustic pressure (dark blue area) on the wavy surface example, which can compromise the probe's ability to detect deeper defects. This test confirms that micrometric variations in the sample waviness generate significant changes in the ultrasonic beam.

After evaluating the impact of surface waviness on the UT beam spread, a defect inspection simulation was performed by introducing two 3 mm diameter flat bottom hole defects, 2.5 mm under the surface, as illustrated on figure 9. Flat bottom holes are a type of reflector commonly used in reference standards where the end (bottom) surface of the hole is the reflector. Defect A is placed under the smooth surface where roughness is the only surface condition, and defect B under a top that complies both roughness and waviness. One can also see the scanning path trajectory which was made over 2 mm steps to minimize computation time, following the x direction.

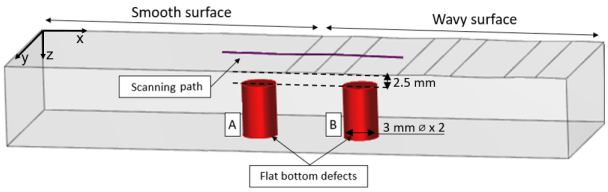

Figure 9: UT inspection model used with two 3 mm diameter flat bottom holes, 2.5 mm under the top surface.

On figure 10, the two defects are shown in their B-scan view. The B-scan refers to the image produced when the data collected from an ultrasonic inspection is plotted on a cross-sectional view of the component. These examples were took by placing the inspection window only over the defects in order to neglect the surface echo to facilitate the comparison.

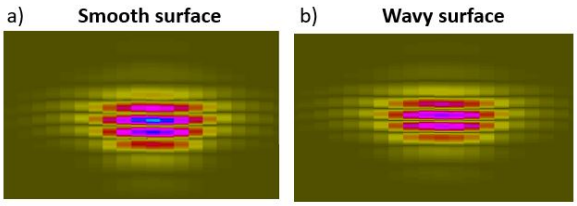

Figure 10: B-scan view of two flat bottom hole defects under different surface conditions.

One can clearly see that both defects appear to have similar acoustic pressure distributions, although there's slight decrease in the wavy surface example. This means that if this decline is significant enough depending on the degree of waviness, the defect detection might be compromised.

Ultimately, the developed model presents a realistic method to understand the effect of surface tex-

ture in the inspection of WAAM parts. This enables a better selection of probes, apertures and other inspection parameters, allowing to predict how the sound pressure behaves within the part. However, this analysis can only be qualitative due to CIVA's comparative scale. For this reason, an experimental validation was followed.

3.2.2 Experimental validation

The followed experiments were made in immersion water coupling with two PAUT probes: an IMASONIC 3.25 MHz with 20 elements plus mechanical focus, and an OIYMPUS 5 MHz with 32 elements. The last was identical to the probe used on CIVA's simulations. Both probes can be seen in figure 11.

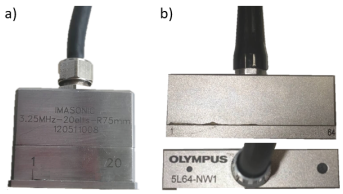

Figure 11: Phased array UT probes used: a) IMASONIC 3.25 MHz 20 elements, b) OIYMPUS 5 MHz 32 elements.

Half of a WAAM wall's top was machined seeking to remove as less material as possible while the other half was kept with its original texture. Two pairs of 3 mm flat bottom holes were placed 4 mm under surface and radiography tests were done to verify the measurements and positioning of the defects, as can be seen in figure 12 a).

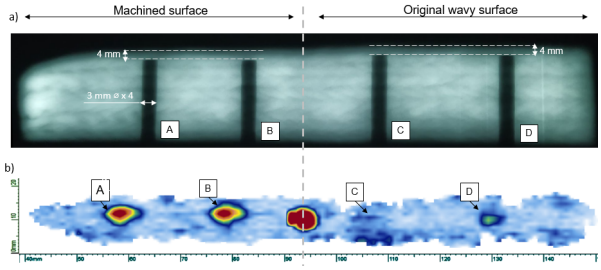

Figure 12: a) Radiography results; b) C-scan view for OLYMPUS 5 MHz probe.

Both 3.25 and 5 MHz probes detected all four defects, but the best and clearer results were achieved with the last for only one active element. Figure 12 b) shows the C-scan of this inspection. A c-scan refers to the image produced when the data collected from an ultrasonic inspection is plotted on a plan view of the component. This last figure shows that defects A and B on the machined half are clearly detected and exhibit very similar acoustic pressure distributions. In contrast, defects C and D on the original wavy side appear more muted. Moreover, defect D is more easily detectable than C which shows that for the inspection of WAAM parts, the defect detectability is highly dependent on the local waviness that the probe encounters.

Defects A and D were selected to be compared and the A-scan results of the first can be seen in figure 13 were the amplitude peak after the first echo clearly exposes the defect.

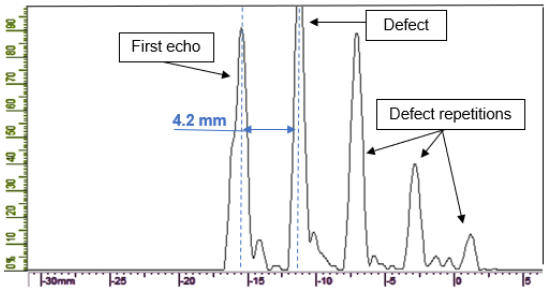

Figure 13: A-scan results for defect A under WAAM surface, inspected with a 5 MHz PAUT probe.

The difference between the peaks of the first echo and the defect was measured indicating a distance of 4.2 mm which is proximate to the real depth of the defect. Although an effort was made to remove as less material as possible while machining, this process also flattened the surface eliminating the characteristic curvature of the samples which might have also contributed for the successful result of this inspection.

Figure 14 shows the A-scan results for defect D under the original wavy surface. As can be seen, the defect was still detected although a general decrease in amplitude is evident compared to defect A on the machined side, as was predicted on the previous simulations. The defect echo amplitude decreased around 80% on the wavy side which is notably significant.

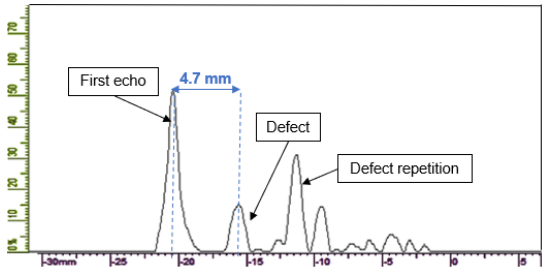

Figure 14: A-scan results for defect D under WAAM surface, inspected with a 5 MHz PAUT probe.

While every defect was able to be detected more or less clearly depending on its localization, there are some considerations to be done relatively to the dimensioning said defects. For defects A and B on the machined half, both could be dimensioned using the same 6 dB rule which is a commonly understood practice for length sizing discontinuities

in welds. This technique defines the defect length as half (6dB) of the maximum amplitude obtained while the transducer is scanned over the flaw. Both holes were measured as having 2.9 mm using this rule, which is acceptable as it is only 0.1 mm away from the real diameter. On the other hand, defect D wasn't able to be correctly dimensioned with the past method, needing a more constricted rule of 3 dB. Defect C was not possible to be dimensioned accurately with any of the mentioned rules, which means that the capabilities of correctly sizing a defect on a typical WAAM surface might be compromised depending on what local waviness the probe encounters.

In conclusion, PAUT proved to be a reliable method for inspecting WAAM steel samples although sizing can be difficult depending on the surface conditions. However, to improve inspection, machining the sample's top might be favorable when applicable.

3.3. Solder paste

When regarding the in-line inspection of WAAM steel parts, there are some challenges concerning coupling that need to be overcome, mostly related to the high temperatures involved in the process. If water is used, it will vaporize instantly at $100°C$ which hinders the chance of active coupling. This problem is even more evident in steel, as temperature cycles can range between 300 - 1150 °C or higher depending on the heat input [5]. One of the solutions for this problem is to increase the cooling time between layers, but that would consequently increase the lead time of manufacturing which is one of the biggest advantages in WAAM [7].

In alternative to water, high temperature UT couplants are usually used in welds, but these tend to leave residues between layers which makes them unsuitable for in-line inspection [LASIMM - internal report]. Therefore, the possibility of using solder paste as UT coupling was tested. The premise was that this paste would be suitable as it formulated to withstand higher temperatures. Moreover, because it is water based, the UT signal should not be compromised.

The conducted tests were done for two samples manufactured with the same welding parameters. The control sample with no solder paste was designated as P1. For sample P2, the solder paste was applied to every layer 1 to 2 minutes after the bead was deposited as to allow some time for cooling to avoid instant vaporization of the liquid. This information is summarized on table 1.

Table 1: Samples production strategy.

Sample	Couplant between layers
P1	-
P2	×

Firstly, it was necessary to understand if the use of the solder past would have any detrimental effect on the microstructure and structural integrity of the WAAM steel parts. To do so, a traversal section of the samples was removed, resin-wrapped and polished. Finally, 2% Nital was used as contrast. The results from a equivalent central portion of both samples are presented on figure 15.

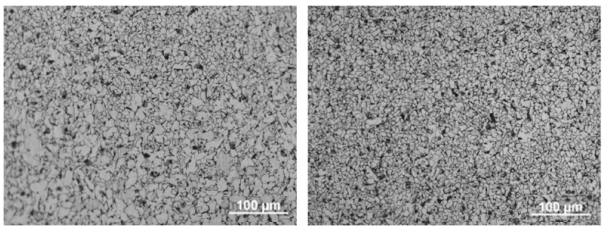

(a) P1 (b) P2

Figure 15: Grain size variation with and without solder paste application.

As can be seen, the main difference observed when comparing the two samples is the grain size. On the sample with solder paste between layers (P2), the grain size is smaller on average and more uniform compared to sample P1. This could be explained by the fact that some of the heat is transferred to the liquid when the paste is being applied, meaning that the welding bead will tend to cool more rapidly. The results are consistent with the theory that rapid cooling is associated to smaller grain formation. Besides grain size variations, neither sample P1 or P2 presented visible defects and similar microconstituents were observed through both samples in equivalent regions. This serves to show that the use of the solder paste does not significantly influence the deposited material at a microstructural level.

Secondly, the mechanical properties of the samples with and without application of the solder paste were studied as they relate to the material's performance. Therefore, tensile and hardness tests were conducted.

Typically, AM produced parts have an oriented grain structure, which means that the mechanical properties can differ in direction. For this reason, the tensile test specimens were removed from the WAAM walls according to the orientation of the build as illustrated on figure 16. These specimens were fabricated following the ISO 6892-1-2009 standard.

The uniaxial tensile tests were performed in a Instron 4507 electromechanically actuated static load frame machine, with a maximum load capacity of 200 kN. Specimens were tested at room temperature using an extensometer to measure

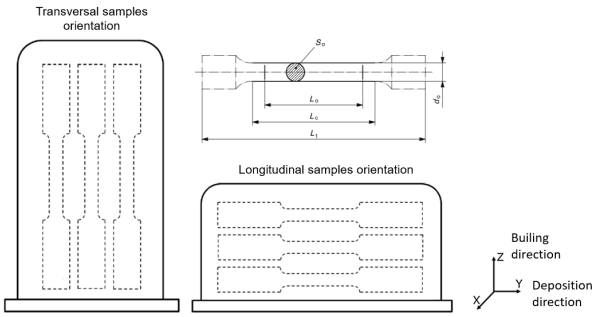

Figure 16: Scheme of the tensile test specimens extracted from WAAM samples according to ISO 6892-1-2009 standard.

changes in the length. The stress-strain curves are shown on figure 17 a) for a more visual examination for 2 pairs of selected specimens. Figure 17 b) shows the statistical representation of all tested specimens. On figure 17 a) the selected stress-

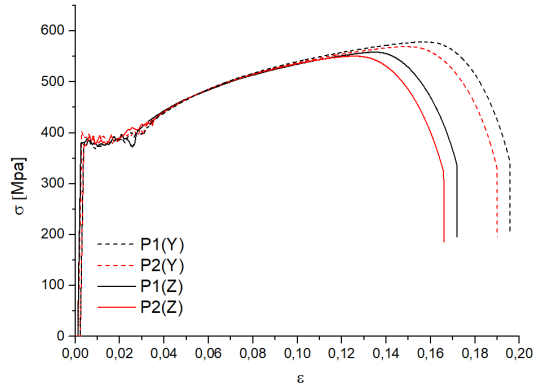

(a) Stress–strain curve.

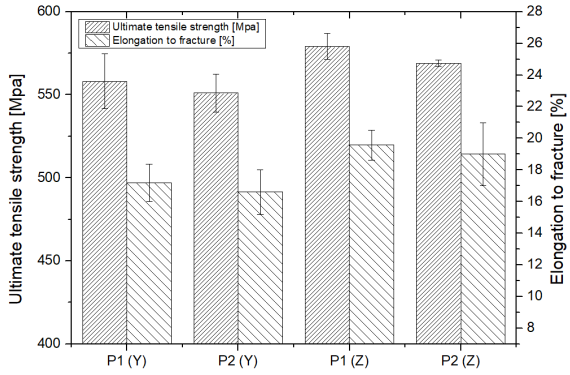

(b) Ultimate tensile strength (UTS) and elongation to fracture of the tested samples.

Figure 17: Tensile test results.

strain curves are representative of a typical mild-steel curve with discontinuous yielding (the material reaches an upper yield point before dropping rapidly to a lower yield point) and ductile behaviour. Some differences can be seen for the transversal (y) and longitudinal (z) components which may be related to preferential orientation of austenite grains during solidification. Ultimately, one can infer that the solder paste usage did not adversely affect the mechanical proprieties of the deposited material.

Finally, hardness tests were conducted by calculating the Vickers Hardenss (VH) along the building direction of the samples using a Duramin Struers machine. The results are presented on figure 18.

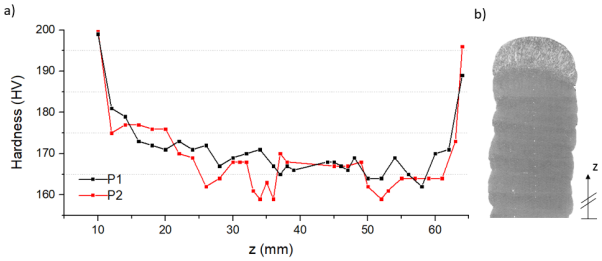

Figure 18: Hardness test results and marked indentations.

Both samples P1 and P2 presented similar behaviour. Although small deviations can be observed, the differences between the peak values are not significant, allowing to conclude that the mechanical properties are homogeneous over each layer, despite variations of the involved temperatures. This was true except for the initial and last layers where the hardness was comparatively higher. The fast cooling rate in the first deposited layers, aided by the cold substrate and its capacity for heat dissipation, justify the higher hardness observed in this region. In the top layers, the microstructure is similar to a single pass weld were acicular ferrite and grain boundary ferrite formation is promoted. This exhibits a predominantly columnar grain structure with relatively higher hardness values.

In brief, the tensile and harness tests revealed similar mechanical behaviour between the samples with and without solder paste, which is a good indicative that its application as couplant will not injure the parts' performance.

Last but not least, scanning electron microscopy (SEM) was conducted in order to verify if the solder paste application had any influence on the chemical composition of the steel samples. The elemental composition of microscopic particles or regions on a sample's surface is analysed using a energy dispersive x-ray spectrometer (EDS) attached to the SEM. EDS micro analysis is performed by measuring the energy and intensity of the signals generated by the focused electron beam scanned across the specimen. The results are shown on figure 19.

These figures show that both samples P1 and P2 had identical chemical composition as the same number of elements were present (C, Mn, Fe, Si) and in approximately the same quantities. This

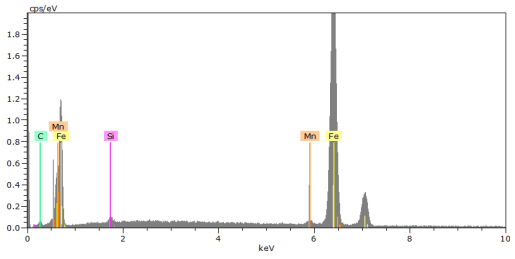

(a) P1.

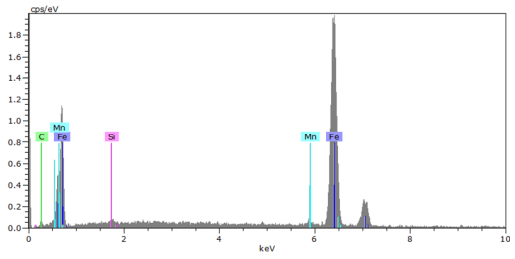

(b) P2.

Figure 19: Elemental composition of the samples.

means that the application of the solder paste did not alter the sample's elemental composition.

3.3.1 Experimental validation

After concluding that the use of the solder paste would not be detrimental to the WAAM steel parts, it was necessary to experimentally validate if this would be a viable couplant for UT. To do so, a conventional 5 MHz UT probe was used on the machined half of the previous UT experiments to inspect the same 3 mm flat bottom hole, 4 mm under surface. The results can be seen in figure 20.

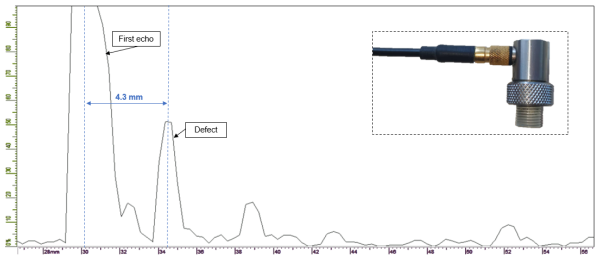

Figure 20: A-scan results for 5 MHz conventional UT probe using solder paste as couplant.

As one can see, the probe clearly defects the defect with a satisfying SNR, proving that the solder paste can be used as an UT coupling similar to water, without compromising the results.

In conclusion, the use of solder paste in ultrasonic coupling shows promising results for the inspection of WAAM steel parts when compared to water or high-temperature couplants as the UT signal was satisfactory and no substantial differences in mechanical behaviour or chemical composition between samples were encountered.

4. Conclusions

The broad goal of this work was to contribute for the quality assurance of parts produced by WAAM using non-destructive techniques. Regarding the first objective of process optimization for surface texture minimization:

- The use of triangular weaving as the deposition strategy was able to significantly decrease the waviness profile down to under 0.01 mm from the oscillation counterpart with 0.045 mm, which indicates a reduction of about 78%.

Concerning the consolidating EC and UT techniques for the detection of internal flaws in steel WAAM parts:

- The new SEP probe design showed improvements over the previous IOnic customized models regarding defect detectability. Thi probe was able to detect a 350 µm x 5 mm internal defect in a carbon steel WAAM sample with acceptable SNR;
- UT inspection showed best results for an OLYMPUS 5 MHz phased array probe. Fat bottom hole defects of 3 mm diameter, 4 mm under surface were detected in a WAAM sample with its original waviness profile;
- Results with a conventional small-footprint 5 MHz OLYMPUS probe show that inspection in WAAM steel samples was unsuccessful in contrast to the same tests performed on aluminium [LASIMM -internal report]. This means that, in the case of steel, phased array should be used when there is no machining between layers;
- The use of solder paste as high temperature UT couplant is promising as it did not adversely interfered with the steel's mechanical proprieties and chemical composition. Experimental results were also successful.

As with most things, an all-purpose solution for the inspection of WAAM parts can't be achieved, as each technique has its own advantages and limitations. For example, UT would be most adequate at the bead intersections than ECT and during the first layers, it would be helpful as the SEP probe needs a certain height to start inspecting due to the lateral excitation format. However, ECT is more adequate for smaller widths compared to the tested phased array probes. This means that the most reasonable inspection should be a combination of both ECT and UT techniques.

For a company that decides to invest in a inline inspection equipment, a thorough investigation

on the part's material, geometrical complexity, and type of defects to inspect must be done *a priori* in order to understand what technique is the most advantageous, if not both.

References

[1] J. B. Bento, A. Lopez, I. Pires, L. Quintino, and T. G. Santos. Non-Destructive Testing for Wire + Arc Additive Manufacturing of aluminium parts. *Additive Manufacturing*, 27:440–450, 2019.

[2] A. Lopez, R. Bacelar, I. Pires, T. G. Santos, J. P. Sousa, and L. Quintino. Non-destructive testing application of radiography and ultrasound for wire and arc additive manufacturing. *Additive Manufacturing*, 21:298–306, 2018.

[3] A. Lopez, J. Santos, J. P. Sousa, T. G. Santos, and L. Quintino. Phased Array Ultrasonic Inspection of Metal Additive Manufacturing Parts. *Journal of Nondestructive Evaluation*, 38:62, 2019.

[4] J. L. Prado-Cerqueira, A. M. Camacho, J. L. Diéguez, Rodríguez-Prieto, A. M. Aragón, C. Lorenzo-Martín, and Yanguas-Gil. Analysis of Favorable Process Conditions for the Manufacturing of Thin-Wall Pieces of Mild Steel Obtained by Wire and Arc Additive. *Materials*, 11:1449, 2018.

[5] T. A. Rodrigues, V. Duarte, R. M. Miranda, T. G. Santos, and J. P. Oliveira. Current Status and Perspectives on Wire and Arc Additive Manufacturing (WAAM). *Materials*, 12:1121, 2019.

[6] P. M. Sequeira Almeida and S. Williams. Innovative Process Model of Ti-6Al-4V Additive Layer Manufacturing Using Cold Metal Transfer (Cmt). *SFF Symposium*, pages 25–36, 2010.

[7] S. W. Williams, F. Martina, A. C. Addison, J. Ding, G. Pardal, and P. Colegrove. Wire + Arc Additive Manufacturing. *Materials Science and Technology*, 32:641–647, 2015.

[8] B. Wu, Z. Pan, D. Ding, D. Cuiuri, H. Li, J. Xu, and J. Norrish. A review of the wire arc additive manufacturing of metals: properties, defects and quality improvement. *Journal of Manufacturing Processes*, 35:127–139, 2018.

[9] J. Xiong, Y. Li, R. Li, and Z. Yin. Influences of process parameters on surface roughness of multi-layer single-pass thin-walled parts in GMAW-based additive manufacturing. *Journal of Materials Processing Technology*, 252:128–136, 2018.